Effects of interface steps on the valley-orbit coupling in a Si/SiGe quantum dot

Bilal Tariq [1,2] and Xuedong Hu[1]

[1]*Department of Physics, University at Buffalo, SUNY, Buffalo, New York 14260, USA*
[2]*National Center for Physics, Quaid-i-Azam University Campus, Islamabad 44000, Pakistan*

Valley-orbit coupling is a key parameter for a silicon quantum dot in determining its suitability for applications in quantum information processing. In this paper we study the effect of interface steps on the magnitude and phase of valley-orbit coupling for an electron in a silicon quantum dot. Within the effective-mass approximation, we find that the location of a step on the interface is important in determining both the magnitude and the phase of the valley-orbit coupling in a Si/SiGe quantum dot. Specifically, our numerical results show that the magnitude of valley-orbit coupling can be suppressed up to 75% by a step of one atomic monolayer, and its phase can change by almost π. When two steps are present, the minimum value of the valley-orbit coupling can even approach zero. Our calculation can in principle be generalized to multiple steps as well, as long as the width of the regions between steps is much larger than the atomistic length scale. We also clarify the effects of an applied external magnetic field and the higher orbital states on the valley-orbit coupling. Overall, our results illustrate that interface roughness can strongly affect both the magnitude and the phase of the valley-orbit coupling, which are crucial parameters for both spin and charge qubits in silicon.

I. INTRODUCTION

Silicon is an ideal host for electron or nuclear spin qubits because of its low abundance of spinful isotopes (which can be further reduced through isotopic enrichment) [1,2]. Extremely long coherence times for both electron and nuclear spins were reported in bulk samples back in the 1950s [3], and were more recently observed in Si nanostructures for single spins [4–7]. There have been multiple experimental demonstrations of high-fidelity quantum gates for single-spin qubits [8–14] and encoded multispin systems [15–24]. The impressive quantum coherence, together with the vast semiconductor industry and its ever improving technological base, makes spin qubits in Si an attractive and promising building block for a future scalable quantum computer.

Significant technological challenges remain toward a fault-tolerant spin qubit in Si, from controlling the effects of charge noise on two-qubit gates to fast and high-fidelity spin measurement. A particular issue of current interest is the consequences of the multivalley structure of the Si conduction band [1,2,25]. The conduction band in bulk Si has six degenerate minima. For electrons confined at an interface four of the valleys have elevated energy so that only two are left in the low-energy sector of the Hilbert space. Scattering at the interface further couples the last two valleys (valley-orbit coupling) and lifts the remaining degeneracy. However this valley splitting tends to be relatively small, about 0.2 to 0.3 meV at a Si/SiO$_2$ interface [26–28] and up to 0.1 meV at a Si/SiGe interface [9–12,17–24], which is usually further reduced by any interface roughness [8,29–31].

The presence of low-energy orbital excited states in a quantum dot (QD) could potentially weaken the foundation for a spin qubit and render it susceptible to leakage and decoherence. Therefore existing experimental and theoretical studies of valley effects have mostly focused on the valley splitting [12,17–23,26–43], with particular interest in how atomic scale features at the interface affect the valley splitting. However, it is important to note that valley-orbit (VO) coupling is in general complex, with its magnitude giving the valley splitting while its phase determines how the valleys are mixed at the interface [32,44]. In a single quantum dot only the magnitude of VO coupling is important, whereas the phase does not have any direct effect on low-energy dynamics. However, in a multidot system both are important to the electron spectra, with the phase in particular a determining factor for all the tunneling matrix elements [20,37,44]. Considering that tunnel coupling is crucial for electron transfer [44–50], charge qubit manipulation [51–55], and exchange coupling between spin qubits [56–58], the phase of the valley-orbit coupling, or more specifically the phase difference between neighboring quantum dots, lies at the foundation for a controllable multiqubit system, and full knowledge of the valley-orbit coupling would be crucial for a complete understanding of the spin and orbital dynamics. Indeed, over the past few years researchers on spin qubits in Si have started exploring the phase aspect of VO coupling [31], and equivalently the intervalley tunnel coupling in the case of a double dot [9,20,35,44,59].

In this paper we study how one or two well-defined interface steps affect both the magnitude and phase of the valley-orbit coupling within the effective-mass approximation. With a single interface step, we find that magnitude of the VO coupling can be reduced by up to 75%, while its phase can vary up to $\sim\pi$. When two interface steps are present and are strategically located, the magnitude of the VO coupling can even vanish completely, while the phase of the VO coupling can vary dramatically depending on where the steps are. In short, our results show that both the magnitude and the phase of the VO coupling are sensitive to the location of the interface

step(s). It is thus inevitable that different quantum dots on the same interface would have different VO couplings if interface steps are present. Such variability in the VO coupling could significantly impact two-dot properties that are important to electron-based quantum information processing, such as tunnel coupling and exchange coupling.

The rest of the paper is organized as follows. In Sec. II we present the theoretical framework of our system and define the Hamiltonians and wave functions of our models. In Sec. III, we calculate the VO coupling for the ground valley states and analyze our results for different geometries described in the previous section. Section IV covers the effect of magnetic field on VO coupling; moreover we discuss the role of excited states on the VO coupling in the ground-state manifold. In the final section we summarize our results and discuss their importance to the experimental study of Si quantum dots.

II. THEORETICAL APPROACH

A. Model Hamiltonian

Typical heterostructures for Si-based quantum computing employ either a silicon oxide or $Si_{1-x}Ge_x$ alloy as a barrier material. The former tends to have a relatively flat interface, while the latter often has a small miscut angle to release the strain built up in the growth process, which in turn results in discrete interface steps. In this work we focus on the Si/SiGe heterostructures, and explore in detail the effects of the interface steps on the electronic states in a single gate-defined quantum dot.

Our model consists of a single electron in a quantum dot with an in-plane (x and y directions) circular confinement of a nominal radius of $\ell_0 = 10$ nm centered at the origin. The out-of-plane confinement is triangular, with a barrier height of U_0, and can be tuned by an applied electric field F. The total Hamiltonian of the electron is $H^{(j)} = H_{xy} + H_z^{(j)}$, with superscript $^{(j)}$ indicating the number of steps at the interface within the quantum dot.

The in-plane part of the one-electron single-dot effective-mass Hamiltonian takes the form

$$H_{xy} = -\frac{\hbar^2}{2m_t}\left(\frac{\partial^2}{\partial x^2} + \frac{\partial^2}{\partial y^2}\right) + \frac{\hbar^2}{2m_t \ell_0^4}(x^2 + y^2), \quad (1)$$

where $m_t = 0.192m_0$ is the transverse effective mass of an electron in Si.

Valley-orbit coupling originates from electron scattering at the interface, governed by H_z. For a smooth interface positioned at z_I, with SiGe in the $z < z_I$ region while Si is in the $z > z_I$ region, the out-of-plane part of the Hamiltonian is

$$H_z^{(0)}(z_I) = -\frac{\hbar^2}{2m_z}\frac{\partial^2}{\partial(z-z_I)^2} + eF(z-z_I) + U_0\theta(z_I - z). \quad (2)$$

Here e is the elementary charge, $m_z = m_l = 0.98m_0$ is the longitudinal effective mass of an electron, F is the interface electric field, and θ is the Heaviside step function. For Si/SiGe $U_0 = 150$ meV. We use an applied electric field $F = 15$ MV/m, as is typical in the literature [30,32].

Within the effective-mass approximation, the electron wave function at a conduction minimum can be written as a product of an envelope function and the underlying Bloch state,

$$D_\xi^{(j)}(\mathbf{r}) = F^{(j)}(\mathbf{r})u_\xi(\mathbf{r})e^{-i\mathbf{k}_\xi \cdot \mathbf{r}}. \quad (3)$$

Here $F^{(j)}(\mathbf{r})$ is the envelope function with the superscript indicating the type of the step(s) at the interface and $u_\xi(\mathbf{r}) = \sum_{\mathbf{K}} c_{\mathbf{K}}^\xi e^{i\mathbf{K}\cdot\mathbf{r}}$ are the Bloch states with $c_{\mathbf{K}}^\xi$ the Bloch coefficients. Here $\xi = \{z, -z\}$ is the valley index, and $\mathbf{k}_\xi = \pm 0.85(2\pi/a_{Si})\hat{z}$ represents the location of the $\pm z$ band minima in the first Brillouin zone of silicon with $a_{Si} = 0.543$ nm being the lattice constant of Si. For a smooth interface the envelope function for the ground state can be further factored into the in-plane and out-of-plane parts: $F^{(0)}(x, y, z) = \phi(x, y)\psi_I(z)$, where $\phi(x, y) = \frac{1}{\pi\sqrt{\ell_0}}e^{-\frac{x^2+y^2}{2\ell_0^2}}$ is the ground state of a two-dimensional harmonic oscillator and $\psi_I(z)$ is the modified Fang-Howard (mFH) wave function along the z direction,

$$\psi_I(z) = Nz_0 e^{\frac{k_b(z-z_I)}{2}}\theta(z_I - z)$$
$$+ N(z - z_I + z_0)e^{-\frac{k_{Si}(z-z_I)}{2}}\theta(z - z_I), \quad (4)$$

where N is the normalization factor. The modified Fang-Howard wave function depends sensitively on the position of the interface z_I [29,60], with k_b determined by the interface potential, z_0 computed from the continuity of the wave function about z_I, and k_{Si} a variational parameter determined by minimizing the electron energy and dependent on the applied electric field along z. For our SiGe barrier, with $U_0 = 150$ meV, $k_{Si} = 0.98$ nm^{-1}.

B. Variational wave function

During the growth process of the Si/SiGe heterostructure, interface steps are inevitable [2,18]. The step heights are an integral multiple of the atomic layer between the Si atoms. For a step of one atomic layer, its height is $d = a_{Si}/4 = 0.136$ nm. In the presence of an idealized straight interface step at $x = x_0$, the z component of the potential is now x dependent,

$$H_z^{(1)}(x_0) = H_z^{(0)}(z_A)\theta(x_0 - x) + H_z^{(0)}(z_B)\theta(x - x_0), \quad (5)$$

where $H_z^{(0)}(z_A)$ and $H_z^{(0)}(z_B)$ are the Hamiltonians given in Eq. (2), with smooth interfaces at z_A and z_B, respectively, as shown in Fig. 1(b).

The effects of an interface step have been considered within the effective-mass approximation before, for example using a smooth tilted interface approximation [17–19]. Here we choose to use the Heaviside theta function to divide the two sides of a step so as to preserve the information on step location, which turns out to be a crucial factor in determining the valley-orbit coupling.

The interface step couples the in-plane and out-of-plane degrees of freedom, making an analytical solution to the electron wave function impossible. We therefore take a variational approach in writing down the envelope function for the QD-confined electron. The main requirement here is to match the modified Fang-Howard wave function with the correct interface position along the z direction because the
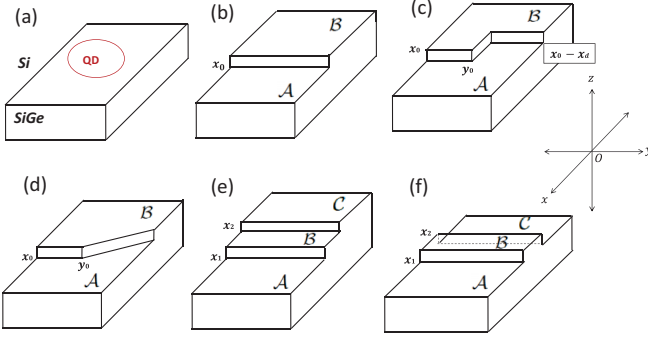
FIG. 1. Schematic representations of different SiGe alloy interfaces that are discussed in this paper.

energy expectation value increases dramatically if there is a mismatch. In the meantime, as an electron crosses an interface step, its z-direction wave function should smoothly shift from one mFH function to another, so that the wave function remains differentiable at all points in space. This smooth transition is achieved by stitching together the mFH functions from regions $\mathcal{A}$ and $\mathcal{B}$ [Fig. 1(b)] using a complementary error function (Erfc) [61].

Consider an example of a single interface step, where we define $\psi_{\mathcal{A}}(z)$ as the ground eigenfunction of Hamiltonian $H_z^{(0)}(z_{\mathcal{A}})$, and $\psi_{\mathcal{B}}(z)$ for $H_z^{(0)}(z_{\mathcal{B}})$. The total envelope function is then

$$F^{(1)}(x_0) = \frac{N_1}{2}\phi(x, y)\left[\psi_{\mathcal{A}}(z)\text{Erfc}\left(\frac{x - x_0}{L_x}\right) + \psi_{\mathcal{B}}(z)\text{Erfc}\left(\frac{x_0 - x}{L_x}\right)\right],$$ (6)

where N_1 is the normalization constant, and L_x is the width of the error function around the step position x_0. L_x is a variational parameter obtained through minimizing the expectation value of the ground-state energy $E^{(1)} = \langle F^{(1)}(r)|H^{(1)}(r)|F^{(1)}(r)\rangle$. For a one-monolayer step we find $L_x = 1.5$ nm, while for a two-monolayer step $L_x = 1.0$ nm. In Appendix A we give a more detailed discussion on L_x.

Interface steps are never truly in a straight line. There are always zigzags along the step as atoms diffuse on the surface during the formation of the interface [62]. We thus also consider two examples as shown in Figs. 1(c) and 1(d), with one having a sharp turn along y while the other has a kink, with the steps on the two sides of the kink extending at different angles. We have also considered an interface with two steps within the range of the quantum dot, as shown in Figs. 1(e) and 1(f). We construct the wave functions in the same manner as in the case of a single step, stitching together wave functions with different interface locations using complementary error functions. Details of the wave functions are discussed in Appendix A.

III. VALLEY-ORBIT COUPLING

The key quantity of interest to us in this study is the valley-orbit coupling, which is defined as

$$\Delta^{(j)} = \langle D_z^{(j)}|V_z^{(j)}(x, z)|D_{-z}^{(j)}\rangle = \left|\Delta^{(j)}\right| e^{-i\phi^{(j)}},$$ (7)

where $V_z^{(j)}(x, z)$ is the interface potential along the z direction. For a smooth interface at $z = z_I$, $V_z^{(j)}(x, z)$ is independent of x and takes the form

$$V_z^{(0)}(z_I) = eF(z - z_I) + U_0\,\theta(z_I - z).$$ (8)

For an interface with one straight step, the potential can be written as

$$V_z^{(1)}(x_0) = V_z^{(0)}(z_{\mathcal{A}})\,\theta(x_0 - x) + V_z^{(0)}(z_{\mathcal{B}})\,\theta(x - x_0).$$ (9)

The more irregular steps can be defined similarly, as discussed in the Appendix A. For two steps,

$$V_z^{(2)}(x, z) = V_z^{(0)}(z_{\mathcal{A}})\,\theta(x_1 - x) + V_z^{(0)}(z_{\mathcal{B}})\,\theta(x - x_1)$$
$$\times \theta(x_2 - x) + V_z^{(0)}(z_{\mathcal{C}})\,\theta(x - x_2).$$

Below we present our results on VO coupling for all cases using the above potentials.

A. VO coupling for a smooth interface

As a benchmark for VO coupling with interface steps, and qualitative understanding on how the phase of VO coupling arises, we first examine the effect of a smooth interface. For an interface at $z = z_I$, we obtain an analytical expression of VO coupling in the absence of umklapp processes by substituting Eq. (3) and Eq. (8) into Eq. (7),

$$\Delta^{(0)} = U_0 c_0^z c_0^{-z*} \frac{N^2 z_0^2}{k_b - 2ik_0} e^{-2ik_0 z_I}.$$ (10)

Here c_0^z and c_0^{-z*} are the Bloch coefficients, for which we adopted values obtained via a density functional theory calculation [33,63]. The magnitude and phase of the VO coupling depends on the strength of the applied electric field along the growth direction via the Fang-Howard parameter k_{Si}, and the location of the interface. For a smooth interface with $F = 15$ MV/m, we have $|\Delta^{(0)}| \sim 0.1$ meV [30,32]. The interface location produces a phase shift, which is a trivial global phase for a smooth interface and can be removed by assuming $z_I = 0$. However, when steps are present, the variations in this phase shift play a crucial role in determining the overall magnitude and phase of the VO coupling.

The phase shift $2k_0 z_I$ arises from electron scattering between the two conduction band minima at $\pm k_0$. With $z_I = 0$ as a reference, the interface at $z_I = \pm d = \pm a_{\text{Si}}/4$ leads to a phase shift of $\pm 2k_0 d$. For a monolayer step, d is one quarter of the Si lattice constant, so that the phase shift is $\pm 0.85\pi$ ($\pm 153°$) (the range of phase is $\{-\pi, \pi\}$). Hence, for step with height $z_I = \pm 2d$, the relative phase is $\pm 0.30\pi$ ($\pm 54°$). This phase shift across an interface step is at the heart of how a step modifies the overall VO coupling at the interface.

B. VO coupling: An interface with one step

Now we calculate the effect of a single interface step on the VO coupling, with particular focus on how the magnitude and phase of the VO coupling depend on the location and height of the step.

Figure 2(a) shows the numerical results of the magnitude of VO coupling as a function of the step position. Clearly, when a step is introduced, it always leads to suppression in the magnitude of the VO coupling because the complex contributions
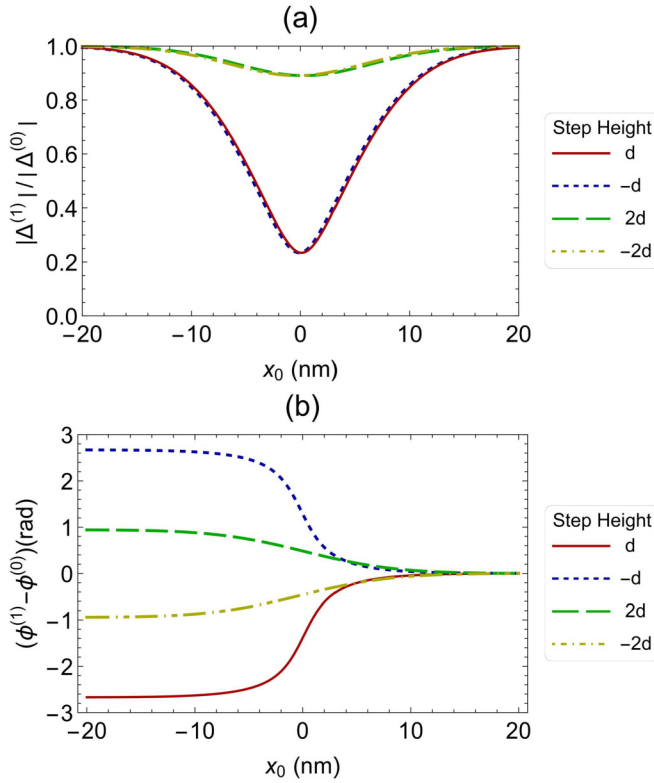
FIG. 2. In (a) we have shown the ratio of magnitude of valley-orbit coupling in the presence of a step to a smooth interface, and in (b) phase change in valley-orbit coupling between interfaces has a step to the smooth interface, as a function of position of step. Here $d = a_{Si}/4 = 0.543$ nm is the monolayer height of the step.

from the two sides of the step [regions $\mathcal{A}$ and $\mathcal{B}$ in Fig. 1(b)] have different phases [19]. For a monolayer step this phase difference is 0.85π. If the step is positioned at the center of the QD, the two regions' contributions to the VO coupling are equal in magnitude but almost opposite in phase, so that they largely cancel each other out. The resulting VO coupling has a magnitude that is only 23% of the smooth-interface value, as shown in Fig. 2(a). When the step moves away from the center of the QD, one region starts to make larger contribution to VO coupling than the other, until the step moves outside the QD, at which point the VO coupling magnitude recovers its smooth-interface value. These results are consistent with the recent tight-binding calculations reported in Ref. [23].

Figure 2(b) shows the phase of the VO coupling as a function of the step position. On the right side of the curve, the phase is zero (by defining that the particular interface location $z_I = 0$) and on the left side the phase is different for the step-up and step-down cases because of the different interface locations, $z_I = \pm d$. The change around the center of the QD is faster than at the edges, which is the consequence of the varying complex contributions from each regions. A change in the QD size along the x direction does not alter the general behavior of the curve in either magnitude or phase, but modifies the width of the changes around the center of the QD. A change in the y dimension has no effect on VO coupling here, while a change in the z dimension brings a change in the VO coupling for a smooth interface, but does

not interfere with the effects of the interface step. It is worth noting that near $x_0 = 0$ (i.e., when the step is close to the center of the dot), a small shift in the step location can lead to a sizable shift in the phase. For example, a shift of x_0 from -2 nm to 0 nm leads to a roughly 0.7 rad (or $40°$) phase shift in the figure (for an electron wave function with a radius of 10 nm). Such a change in phase could significantly impact physical quantities that depend on the interdot VO coupling phase difference, such as interdot tunneling [44].

Under certain experimental conditions, interface steps may become bunched during the growth process [64] and the resulting step height is of two atomic layers. Now the phase change across the step is $4k_0d = 1.7\pi = 306°$, which is equivalent to $-0.3\pi = -54°$. This phase difference is much less than the single-monolayer case, so that the suppression in the magnitude of VO coupling is now less severe. The minimum value for VO coupling still occurs at the center of the QD, though the reduction is only about 10% of the original value. The phase varies from 0 to $\pm 54°$ as shown in Fig. 2(b), with the step-up and step-down cases opposite in their trends.

Considering that each contribution to the VO coupling from a particular step region is a complex number and can be represented by a two-dimensional vector, our results can be explained using a simple vector model. Mathematically, the VO coupling defined in Eq. (7) can be expressed as follows in the presence of an interface step and neglecting the overlapping contributions from the two sides of the step (assuming the complementary error function as a step function since $L_x \ll \ell_0$):

$$
\begin{aligned}
\Delta^{(1)} &\approx \Sigma_0 \int dxdydz\, e^{-2ik_0z} |\phi(x,y)|^2 \psi_{\mathcal{A}}(z)^2 \theta(x_0 - x) \\
&+ \Sigma_0 \int dxdydz\, e^{-2ik_0z} |\phi(x,y)|^2 \psi_{\mathcal{B}}(z)^2 \theta(x - x_0) \\
&\approx \frac{\Delta_0}{a\sqrt{\pi}} \Bigg[\int_{-\infty}^{\infty} dx\, e^{-\frac{x^2}{a^2}} \theta(x_0 - x) \\
&+ e^{-2ik_0(z_B - z_A)} \int_{-\infty}^{\infty} dx\, e^{-\frac{x^2}{a^2}} \theta(x - x_0) \Bigg] \\
&= \Delta_{\mathcal{A}} + \Delta_{\mathcal{B}},
\end{aligned}
\tag{11}
$$

where $\Sigma_0 = U_0 c_0^z c_0^{z*}$. In the last expression above each term can be assigned a two-dimensional vector. The first vector represents a contribution from region $\mathcal{A}$, the second vector region $\mathcal{B}$. The magnitude of a vector is given by the electron probability in the corresponding region, while the relative direction of the vectors given by the phase $e^{-2ik_0(z_B - z_A)}$.

For the two interface regions $\mathcal{A}$ and $\mathcal{B}$ in Figs. 1(b)–1(d), we associate each as a vectors with the following properties:

(1) The direction of each vector is fixed by the corresponding z_I, as $-2ik_0z_I$ measured from the x axis.

(2) The magnitude of each vector depends on the fraction of electron probability within the specific step region in the QD.

(3) The algebraic sum of the magnitudes of all the vectors is a constant (for one step here $|\Delta_{\mathcal{A}}| + |\Delta_{\mathcal{B}}| = |\Delta^{(0)}|$), reflecting normalization of the electron wave function.

Consider the example of a step at the center of the quantum dot. Here the vectors from the two sides of the step have the same magnitude ($|\Delta_{\mathcal{A}}| = |\Delta_{\mathcal{B}}| = |\Delta^{(0)}|/2$) but are directed at

different angles. The relative angle between the vectors for a monolayer step is $153°$. Hence the ratio of the magnitude should be $|\frac{1}{2}(1 + e^{-i0.85\pi})| = 0.23$, consistent with our numerical calculation. When the step moves away from the center, the magnitudes of the two vectors increase and decrease with the same pace and can be represented as $|\Delta_{\mathcal{A}}| + \delta$ and $|\Delta_{\mathcal{B}}| - \delta$. Assuming the phases of the two contributions to be 0 and θ, the sum $\Delta^{(1)}$ of these two vectors/complex numbers can be expressed as $\Delta^{(1)} = (|\Delta_{\mathcal{A}}| + \delta) + (|\Delta_{\mathcal{B}}| - \delta)e^{i\theta}$. Its magnitude is

$$|\Delta^{(1)}| = \sqrt{\frac{|\Delta^{(0)}|^2}{2} + 2\delta^2 + 2\left(\frac{|\Delta^{(0)}|^2}{4} - \delta^2\right)\cos\theta}, \quad (12)$$

which is an even function of δ (which in turn is proportional to the step location measured from the center of the dot). $|\Delta^{(1)}|$ also only depends on $\cos\theta$, so that the sign of θ does not matter, which implies that the VO couplings for the step-up and step-down situations should have the same magnitude. The phase of the sum is given by

$$\tan\phi = \frac{(|\Delta^{(0)}| - 2\delta)\sin\theta}{|\Delta^{(0)}| + 2\delta + (|\Delta^{(0)}| - 2\delta)\cos\theta}, \quad (13)$$

which approaches 0 when $\delta \to -|\Delta^{(0)}|/2$ (smooth interface with $z_I = 0$) and θ when $\delta \to |\Delta^{(0)}|/2$ (smooth interface with z_I a constant of d or $2d$). Therefore, our results presented above can be almost exactly represented by the behavior of the sum vector $\Delta^{(1)}$.

C. VO coupling: Irregular one step

With wave function overlap negligible across a step, the VO coupling is mostly determined by the contributions from different regions proportional to their respective areas within the QD range, as illustrated by the excellent agreement between our simple vector model and the numerical results for a single straight step above. Within this model, the shape of the step also does not matter. To demonstrate this point, we introduce two irregular steps, one with a straight step along the y direction but with a sharp zigzag turn along the x direction [Fig. 1(c)], and the other with two segments that are at an angle between each other [Fig. 1(d)].

Figure 3 presents the results of the zigzag turn case, with the VO coupling as a function of variables x_d (the length of the x-direction segment) and y_0 (the location of the zigzag). $y_0 = -20$ nm represents the point where the zigzag is below the QD so that there is only a straight step through the QD. This is thus similar to the straight-step case. In particular, when $x_d = 0$ we get a suppressed VO coupling of 23% magnitude, the same as before, and the phase is also the same as expected. Hence, we see similar results to one step for both magnitude and phase. At $y_0 = 0$ for $x_d = 10$ nm, the area occupied by region $\mathcal{A}$ is three quarters whereas that for region $\mathcal{B}$ is one quarter. They both will add-up with the phase factor and give the result of approximately 50% change in magnitude. This case is symmetric when region $\mathcal{B}$ occupies three quarters and region $\mathcal{A}$ one quarter. On the other hand, when $y_0 = 20$ nm the change of x_d does not affect the VO coupling. The changes happen outside the dimensions of the QD and we see no change in the result.
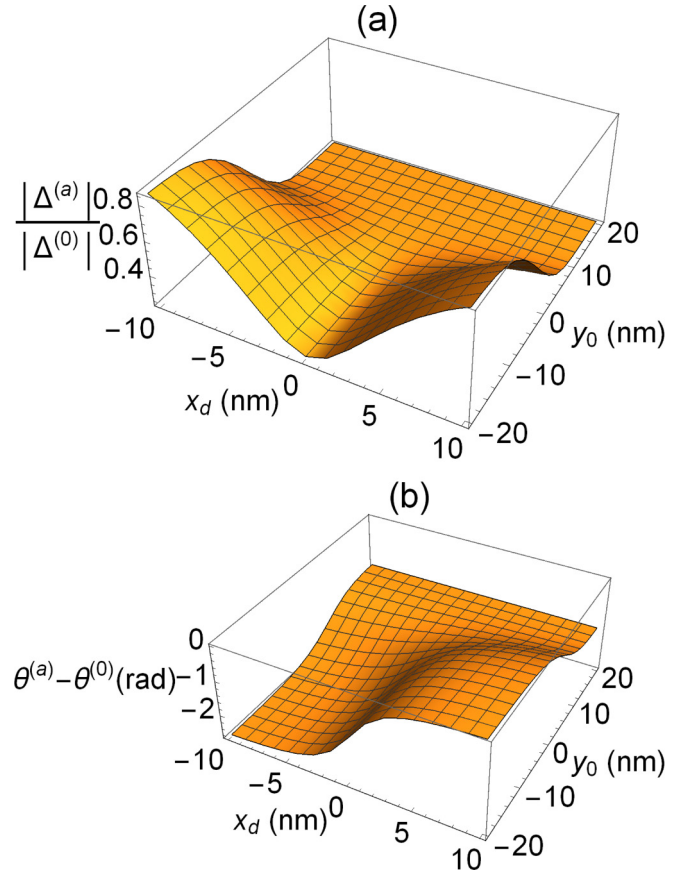
FIG. 3. Three-dimensional plot of the ratios of magnitudes in (a) and phase differences in (b) of VO coupling as a function of positions of the step at y_0 and a sharp turn of width x_d in the x direction.

For the angled-turn case shown in Fig. 1(d), we take y_0 to be fixed at the center of the QD and study the VO coupling's dependence on the turning angle θ. For example, when $\theta = -\pi/2$, region $\mathcal{A}$ occupies three-fourths of the total area of the QD, while region $\mathcal{B}$ occupies one-fourth. The results presented in Fig. 4, for both magnitude and phase of the VO coupling, are the same as in Fig. 3. In short, the results illustrate again our point that it is the area of each region, not the shape of the boundary, that is the determining factor for the overall VO coupling.

D. VO coupling for an interface with two steps

When two straight steps are present on an interface, the VO coupling in a QD is the sum of contributions from three step regions labeled as $\mathcal{A}$, $\mathcal{B}$, and $\mathcal{C}$, as illustrated in Figs. 1(e) and 1(f). These regions differ by the z position of the barrier potential between Si and SiGe. There are four possible geometrical combinations: stairs (upward or downward) and rectangular terraces (normal or inverted), as discussed in Appendix A 3. The VO couplings of stairs-up and stairs-down cases are differentiated only through their phases, similarly to the one-step case. Without loss of generality, we focus on the stairs-up and rectangular-terrace cases in the following calculations and discussion.
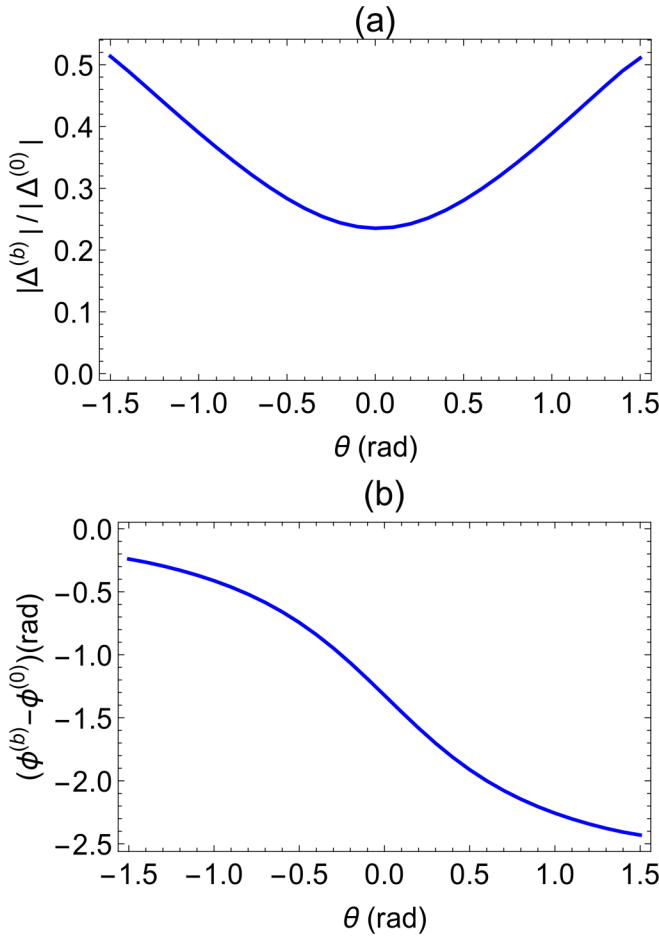
FIG. 4. Magnitude (a) and phase (b) of VO coupling as a function of tilt angle (θ) for geometry given in Fig. 1(c). We fixed $x_0 = 0$ and $y_0 = 0$, i.e., at the center of the QD.

1. VO *coupling for stairs*

Figure 5 shows the results of both magnitude and phase of the VO couplings as functions of the locations of the two steps in a stair configuration. The most prominent feature for the magnitude of VO coupling here is that it can actually reach zero for a specific set of step locations, when the steps are at $x_1 = x_{10} = -4.4$ nm and $x_2 = x_{20} = -x_{10} = 4.4$ nm (recall that the radius of the QD is 10 nm). While the chance of getting such a step configuration is small in a real QD, the VO coupling could be strongly suppressed if the two steps are close to this configuration.

Physically, at this particular step configuration, the contributions from each region toward the VO coupling cancel one another because of their phase differences. Within our vector model, if we let $\Delta_{\mathcal{A}} = |\Delta_{\mathcal{A}}|e^{-i\theta}$, $\Delta_{\mathcal{B}} = |\Delta_{\mathcal{B}}|$, and $\Delta_{\mathcal{C}} = |\Delta_{\mathcal{C}}|e^{i\theta}$ represent the contributions from each of the step regions, with $\theta = 0.85\pi$, the condition for a complete cancellation of the VO coupling in the QD is

$$|\Delta_{\mathcal{A}}| = |\Delta_{\mathcal{C}}| = \frac{|\Delta^{(0)}|}{2(1 - \cos\theta)}, \tag{14}$$

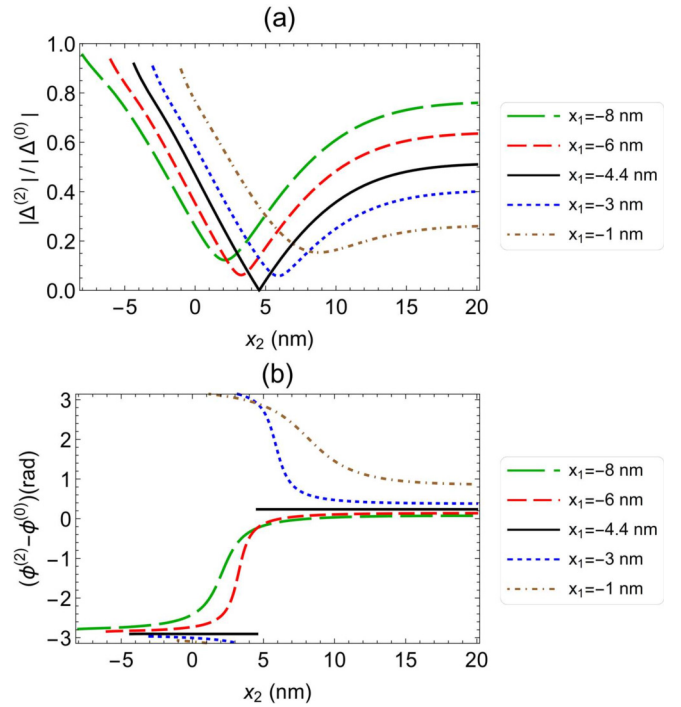$$|\Delta_{\mathcal{B}}| = -\frac{|\Delta^{(0)}|\cos\theta}{1 - \cos\theta}, \tag{15}$$

FIG. 5. Magnitude ratios and phase differences for a staircase with each step of height one monolayer as a function of second step. We use different fixed positions of the first step and the position of step two begins from first-step location.

with the magnitude of each contribution linearly proportional to the electron probability in the respective step region, which is roughly proportional to the area of the region within the QD. Quantitatively, the middle step should occupy about 47% of the electron probability in the QD, while the other two steps split the rest.

The phase of the VO coupling is ill defined when its magnitude vanishes, and could have a discontinuity as we change the step configurations. This is indeed the case as shown by the black solid line in Fig. 5(b), which represents the configurations with $x_1 = x_{10}$ while x_2 is varied around x_{20}. Somewhat surprisingly, in this case the phase has only two values that differ by π. This feature can again be explained within our vector model. Qualitatively, when x_1 is fixed at x_{10}, the total vector changes only its magnitude but not its angle when x_2 is varied. When x_2 sweeps past x_{20}, the vector simply flips its direction, so that the corresponding complex number changes its phase by π. For a more detailed discussion please see Appendix C.

Doubling the height of each step (Fig. 6) changes the phases of regions $\mathcal{A}$ and $\mathcal{C}$ to $\pm 4k_0 d = \mp 0.3\pi$ (assuming the phase of the region $\mathcal{B}$ contribution is 0). Now the overall VO coupling cannot vanish anymore, and generally has much larger magnitude than the case of two single-monolayer steps. The minimum magnitude occurs when the two steps merge at the center of the QD with a height of $4d$, with the value of $|\frac{1}{2}(1 + e^{-4i0.85\pi})| = 0.59$. As the second step moves outside the dot the magnitude of VO coupling gets the value of one step with height $2d$. The phase of the VO coupling smoothly shifts from the case of a step of height $4d$ to a height of $2d$. In
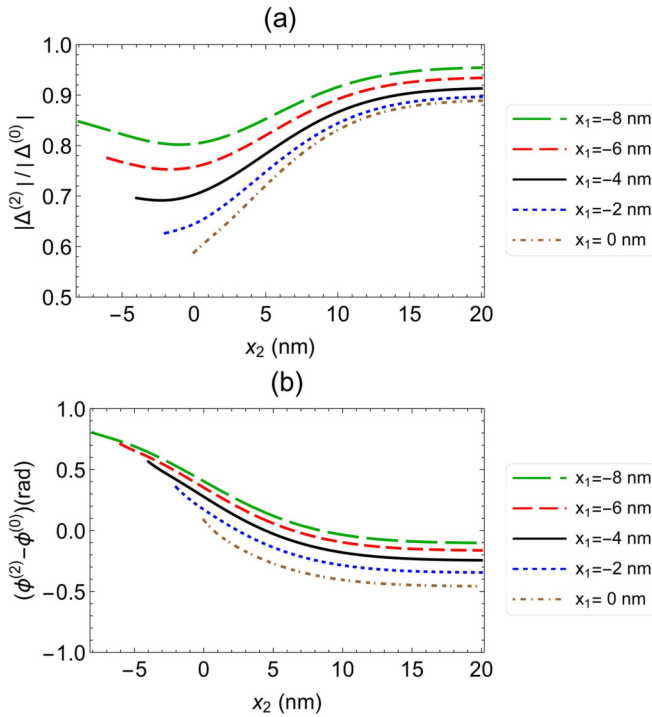
FIG. 6. Results of magnitude ratios and phase differences for stair case with each step of height $2d$ for several fixed locations of first step as a function of second-step position.
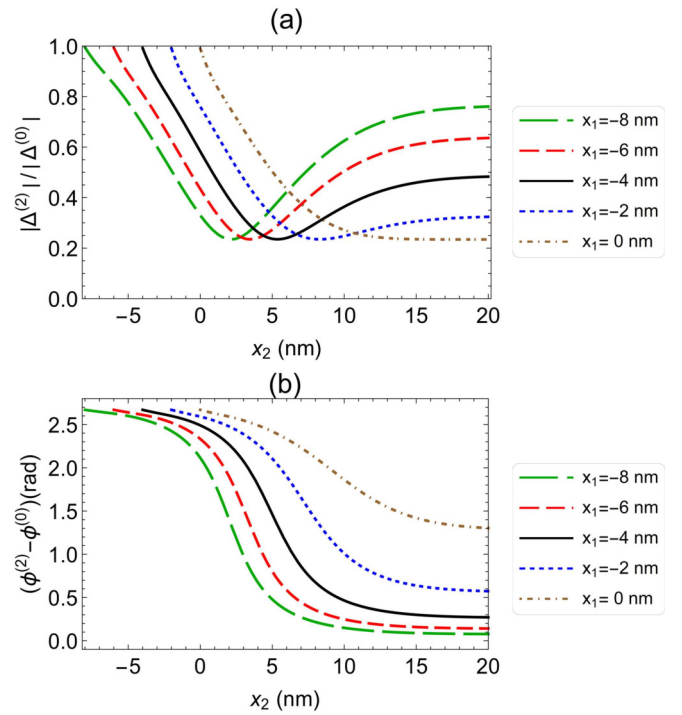

FIG. 7. Magnitude ratios and phase differences for rectangular terrace of height one monolayer, d, as a function of second step. We use different fixed positions of the first step and the position of step two begins from first-step location.

terms of the vector notation, here the magnitude of total VO coupling never goes to zero, and there is no discontinuity in its phase.

2. VO *coupling in rectangular terraces*

When a rectangular terrace is present on the interface (a step up followed by a step down), the magnitude of VO coupling has a nonzero minimum value just like in the single-step case. Furthermore, this minimum value is identical to the value obtained in the single-step case as well. In Fig. 7(a) we show some numerical results for different terrace configurations, with five different locations of the first step on the left side of the quantum dot. The second step position always satisfies $x_2 > x_1$. Each of the curves starts from 1 when the two steps are on top of each other so that the terrace is absent. As the second step moves away from the first step, the value of the magnitude of VO coupling drops to a minimum value and then goes back up again. No matter where x_1 is (as long as $x_1 < 0$), the minimum value of the VO coupling remains the same. As for the phase of the VO coupling, for each x_1 the phase starts from zero when both steps are at the same point and there is no terrace. The contribution from the terrace increases as x_2 moves away from x_1 and the terrace area becomes larger. Finally, when the second step moves outside the QD we recover the single-step case (with step location at x_1) as shown in Fig. 2(b).

These results can be interpreted by our vector model straightforwardly. As in the case of a stair, here the contributions to the VO coupling again come from three regions, labeled as $\mathcal{A}$, $\mathcal{B}$, and $\mathcal{C}$. What is different here is that regions $\mathcal{A}$ and $\mathcal{C}$ have the same location for the interface, so that the

vectors representing these two regions are aligned and can be combined into a single vector, whereas the contribution from region $\mathcal{B}$ is at an angle 0.85π from those of $\mathcal{A}$ and $\mathcal{C}$. Clearly, the sum of these three vectors (practically two if $\mathcal{A}$ and $\mathcal{C}$ are combined) would never vanish. Writing the total VO coupling as $\Delta^{(2)} = \Delta_{\mathcal{A}} + \Delta_{\mathcal{B}} + \Delta_{\mathcal{C}} = |\Delta_{\mathcal{B}}| + (|\Delta_{\mathcal{A}}| + |\Delta_{\mathcal{C}}|)e^{-i\theta}$, and knowing that $|\Delta_{\mathcal{A}}| + |\Delta_{\mathcal{B}}| + |\Delta_{\mathcal{C}}| = |\Delta^{(0)}|$ is a constant determined by the QD area, we can easily find that the minimum of $|\Delta^{(2)}|$ happens when $|\Delta_{\mathcal{B}}| = \frac{1}{2}|\Delta^{(0)}|$ irrespective of what the split is between regions $\mathcal{A}$ and $\mathcal{C}$, and the value of the minimum is $|\Delta^{(2)}| \sim 0.23|\Delta_0|$, the same as in the single-step case. Again, from the perspective of this model, the key factor is the electron probability distribution among the different step regions within the QD, not exactly where the terrace is.

If the terrace step height is $2d$ (two atomic monolayers; Fig. 8), the magnitude of the VO coupling follows the same trend as above, albeit with a smaller overall magnitude in modification, consistent with what we observed in the single-step case. The phase also follows the same trend as in the single-step case (the $-2d$ dot-dashed curve in Fig. 2), as would be predicted by our vector model.

Our results on two-step interfaces show that both the magnitude and phase of the valley-orbit coupling in a Si quantum dot are dependent on the configurations of the steps. In particular, when the two steps are in a stair formation, the VO coupling can be completely suppressed for a specific combination of step locations. However, digging beneath the surface, our effective-mass model also indicates that it is the electron probabilities in each step region within the QD
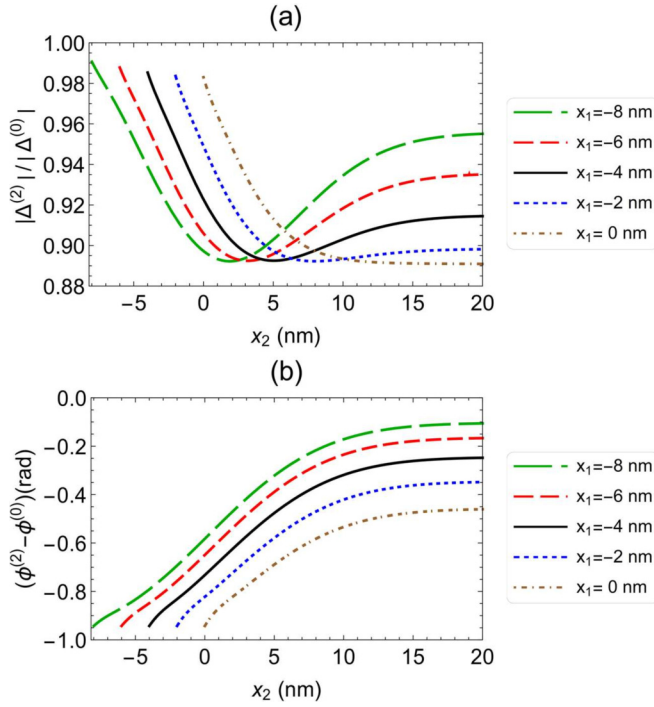
FIG. 8. Results of magnitude ratios and phase differences for rectangular terrace of height $2d$ for several fixed locations of first step as a function of second-step position.
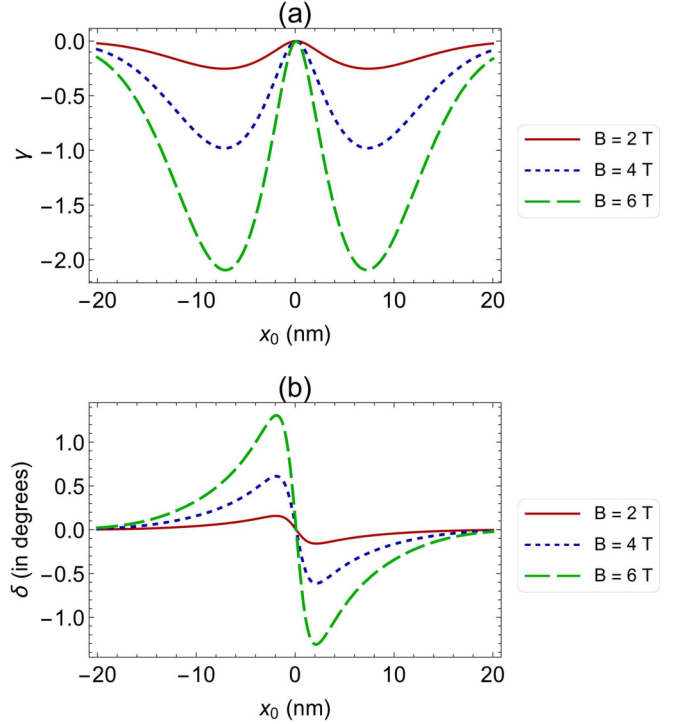

FIG. 9. In (a) and (b) we show the percentage difference in magnitude and difference in the phase of the VO coupling given in Eqs. (17) and (18), respectively, for three different values of magnetic field as a function of step location.

that determines the behavior of the overall VO coupling. For example for the cases of terraces, the VO coupling would be minimized as long as half of the electron probability is within the terrace, no matter exactly where the terrace is within the QD's geometric shape.

In general, the effective-mass calculation performed here, and the vector model we use to explain our results, can be generalized to interfaces with many steps, as long as the terraces between steps are much broader than the atomistic length. If these terraces are too narrow, contributions from neighboring terraces cannot be neglected (recall that our variational step width parameter takes the value of 1.5 nm) and the envelope function approximation starts to break down. At this limit of atomistic scale interface roughness, a tight-binding calculation that can access the small length scale would be more appropriate.

IV. EFFECTS OF MAGNETIC FIELD AND HIGHER ORBITAL STATES ON THE GROUND-STATE VALLEY-ORBIT COUPLING

So far in this study our key observation is that in the case of a relatively smooth interface with one or two steps, the crucial factor in determining the magnitude and phase of the VO coupling is the area/electron probability of each step (with a particular interface location z_I) within a quantum dot. There is no direct contribution from the step edge within our effective-mass model.

When a magnetic field is applied along the growth direction of a two-dimensional quantum dot, it causes a stronger

confinement and a reduction in the Fock-Darwin radius of the electron wave function (i.e., the characteristic length of the electron wave function) [57],

$$\ell(B) = \ell_0 \left[1 + \frac{1}{4} \left(\frac{\ell_0}{\ell_B} \right)^4 \right]^{-\frac{1}{4}}, \tag{16}$$

where ℓ_0 is the radius of the ground Fock-Darwin electron state at $B = 0$, and $\ell_B = \sqrt{\frac{\hbar}{eB}}$ is the magnetic length for the applied magnetic field along the z direction. Such a change in the size of a QD could theoretically shift the position of a step relative to the center of the QD, therefore leading to changes in the VO coupling. However, since the Si QD radius is generally quite small (we have used a nominal value of 10 nm in this study), this magnetic confinement effect turns out to be negligible. Benchmarked against the zero-field results, the quantities of interest here are the percentage difference in the magnitude of VO coupling and overall phase shift,

$$\gamma = \frac{|\Delta^{(1)}(B)| - |\Delta^{(1)}(B = 0)|}{|\Delta^{(0)}(B = 0)|} \times 100\%, \tag{17}$$

$$\delta = \phi^{(1)}(B) - \phi^{(1)}(B = 0). \tag{18}$$

In Fig. 9(a), we indeed observe a very small change in VO coupling as a function of the magnetic field [65], in the presence of a single step because of the relatively small change in the confinement radius: the largest change is 4.6%, at $B = 6$ T. There is no change in VO coupling if the step is at the center of the QD because the magnetic field does not shift the electron
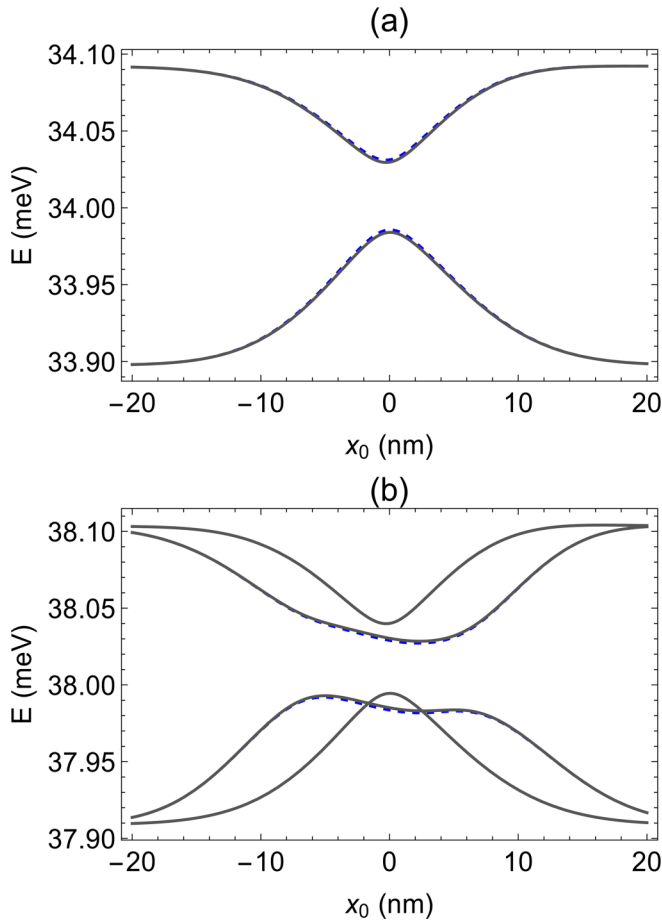
FIG. 10. The ground and the first excited state energy spectrum as a function of step position are shown in (a) and (b), respectively. The solid line curves represent the results which include the coupling between s and p states and the dashed line approximates results with the exclusion of coupling between s and p states.

FIG. 11. Percentage difference in VO coupling for ground state in the presence of p as a function of step position.

valleys. The basis is $\{D_{z,s}^{(1)}, D_{-z,s}^{(1)}, D_{z,p_x}^{(1)}, D_{-z,p_x}^{(1)}, D_{z,p_y}^{(1)}, D_{-z,p_y}^{(1)}\}$. Qualitatively, the presence of a step on the interface breaks the symmetry of the Hamiltonian along the x direction, resulting in a coupling between the ground and the excited p_x states.

The effective Hamiltonian within the s-p subspace can be represented as

$$H = \begin{bmatrix} H_{ss} & H_{sp} \\ H_{ps} & H_{pp} \end{bmatrix}.$$

Here the blocks H_{ss} and H_{pp} represent the ground and first excited orbital state manifolds (assuming valley splitting is much smaller than the orbital excitation energy) and H_{sp} and H_{ps} are the coupling between the ground and excited states. We diagonalize this matrix and plot the energy spectrum in Fig. 10. We have also included results when assuming $H_{ps} = H_{sp} = 0$, and observe a very small change as shown by the dotted lines in Fig. 10. In Fig. 11 we plot the percentage change in the VO coupling in the presence of the excited state as compared to ground-state-only results. Clearly, the contribution from the excited states on the VO coupling in the ground state is negligible, and our ground-state-only calculation above is justified.

V. CONCLUSION

In conclusion, we have calculated the valley-orbit coupling in a Si/SiGe quantum dot in the presence of interface steps. We employ a variational approach within the effective-mass approximation for this calculation. Our results show that the presence of interface steps could lead to significant suppression of the magnitude of the VO coupling, and cause large phase shift (up to π) to the VO coupling. Our results can be explained by the assumption that the overall VO coupling is the sum of contributions from individual step surfaces. The phase of an individual contribution is determined by the interface position of the step along the growth direction, while its magnitude is determined by the electron probability on the particular step enclosed within the QD. This model can be visualized using vectors to represent the individual step surface contributions, with the sum of the magnitude of the vectors a constant and the direction of each vector fixed. We have also explored the effects of an external magnetic field and the excited orbit states, and find both to have only minor

wave function. The phase of the VO coupling has a similarly very weak dependence on the magnetic field, as shown in Fig. 9(b). As we mentioned before, this weak dependence on the applied magnetic field is to be expected. Indeed, given a 10 nm zero-field radius for the electron ground state, we have a total confinement radius for different values of the B field as $\ell(2\,\mathrm{T}) = 9.94$ nm, $\ell(4\,\mathrm{T}) = 9.78$ nm, and $\ell(6\,\mathrm{T}) = 9.54$ nm. Even at 6 T, the confinement length is still only modified by 5%. It is therefore not surprising that the field does not cause the step location to change within the QD, so that VO coupling is not affected significantly by a magnetic field.

Our results so far indicate that the determining factor in the calculation of the VO coupling in the presence of interface steps is the electron probability in each step region within the QD. With our calculations based on a variational ground-state wave function, it is important to establish its validity by clarifying whether the steps cause significant scattering between the ground and excited orbital states.

This can be done by introducing the higher-energy p states in our calculations with a single interface step. Now the low-energy Hilbert subspace comprises the ground state and a twofold-degenerate excited orbital state [66], in addition to the
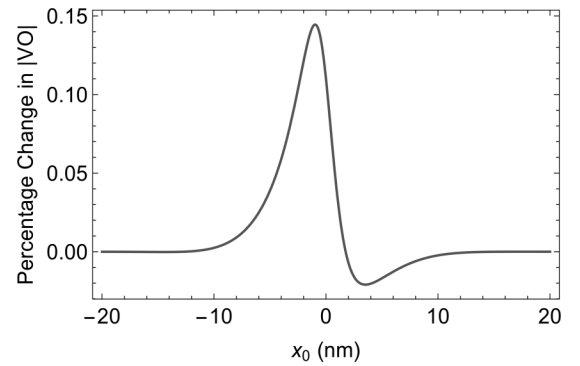
effects. Our results on the magnitude of the VO coupling are consistent with results reported in the literature, while our results on the phase of the VO coupling should be a useful guideline when exploring variations in the interdot tunneling and exchange coupling in double and multiple quantum dots.

In this work we have systematically examined the dependence of the complex VO coupling in a single quantum dot on the presence of interface steps. As we have discussed in the introduction, a clear understanding of both the phase and magnitude of VO coupling is essential in the case of a double or multiple quantum dot. For example, a phase difference between neighboring quantum dots means that tunneling between different valleys are allowed [44], while a smooth interface would have only allowed tunneling between the same valley eigenstates. The modified single-electron tunneling in turn would affect the exchange coupling between neighboring electrons, which are proportional to the square of tunnel couplings. We are currently exploring these effects and how they could impact spin and charge qubits in Si, and the results will be presented elsewhere.

APPENDIX A: VARIATIONAL WAVE FUNCTIONS

1. How to determine L_x

As discussed in the main text, in the presence of an interface step, we assume that the growth direction electron wave function on each step surface takes the modified Fang-Howard form. To ensure that the wave function is continuous across a step, we stitch the two modified Fang-Howard functions together using the complementary error function:

$$\mathrm{Erfc}(\beta) = \frac{2}{\sqrt{\pi}} \int_{-\infty}^{\beta} e^{-t^2}\, dt,$$

where $\beta = \frac{x - x_0}{L_x}$, x_0 is the position of the step in the x direction, and L_x represents the width of the error function. L_x thus dictates how smooth the wave function transition is. We treat L_x as a variational parameter and calculate it by minimizing the energy of the ground state:

$$E^{(1)} = \langle F^{(1)}(r)|H^{(1)}(r)|F^{(1)}(r)\rangle.$$

The expectation value here depends on the location and height of the step as well as the width of the error function. For a given height of the step, the optimal L_x varies with the position of the step. In our calculation reported in this paper, we choose three values of x_0 near the center of the QD, calculate the optimal value of L_x, and then average over them. For the values of x_0 used in Fig. 12, we obtain $L_x = 1.5$ nm. Notice that while the value of L_x is important in calculating the total energy of a state, it has no significant impact on the calculation of the VO coupling as we discuss below.

We observe in Fig. 12 that the variation in energy for the one-step case is small if we vary the L_x within 1 to 2 nm,
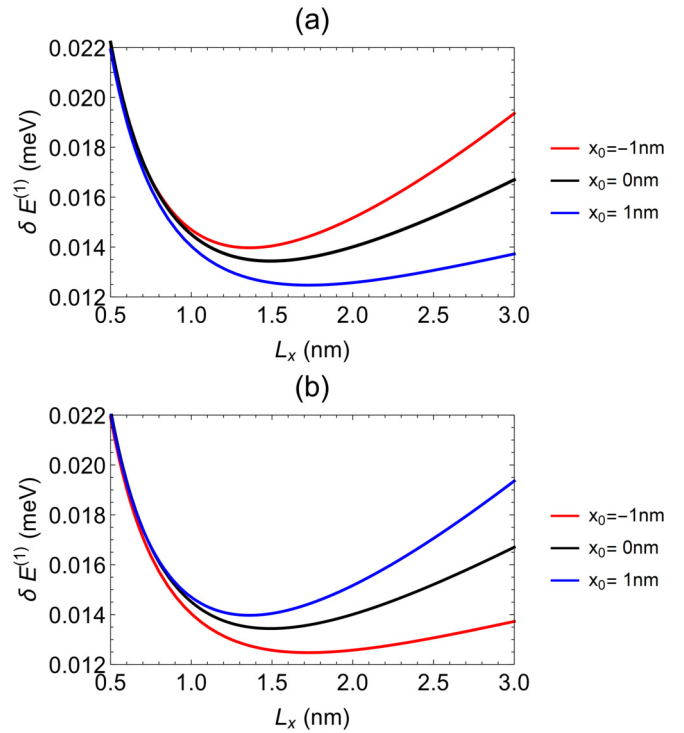

FIG. 12. Change in the expectation value of energy $(E^{(1)} - E^{(0)})$ in the presence of (a) step up and (b) step down as a function of a variational parameter, the width of the complementary error function L_x. We consider three locations of the step close to the center of the QD.

whereas outside this range the change in energy is more dramatic. Most importantly, we find that for the one-step case the value of L_x (e.g., 0.5 nm and 5 nm, respectively) has minimal effect on the VO coupling, as shown in Fig. 13. In other words, the approximate nature of our choice of L_x does not affect the objective of evaluating the VO coupling.

When excited states are included in our calculation, we adopt the same approach in stitching together the growth-direction wave functions across a step. For these states the optimal value of L_x is not necessarily the same as that for the ground state. Nevertheless, we adopt the same L_x for the p states (Fig. 14), and observe through numerical calculation that their effect on the ground-state VO coupling is less than 0.15 percent. It is thus safe to neglect the effects of the higher-energy orbital states, as we have done in the calculations presented in the main text.
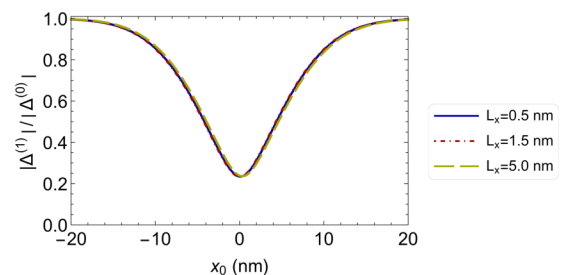

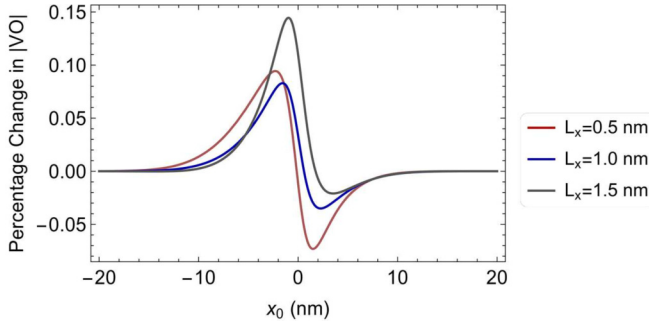FIG. 13. Effect of L_x on VO coupling.

FIG. 14. Percentage difference in VO coupling in the ground state in the presence of p from when there is only the s state for different values of L_x.

2. Variational wave function: Irregular one step

On a realistic interface, a step is never a straight line. To model irregular shapes of an interface step, we consider two examples as shown in Figs. 1(d) and 1(e), with one having a sharp zigzag turn along the y direction and the other having two segments at an angle with respect to each other. The Hamiltonians for the two cases are

$$H_z^{(a/b)} = H_z^{(1)}(x_0)\,\theta(y_0 - y) + H_z^{(1)}(x_0 + x^{(a/b)})\,\theta(y - y_0), \tag{A1}$$

where $H_z^{(1)}(x_0)$ is given in Eq. (5), and the corresponding wave functions are given as

$$F^{(a/b)}(y_0) = \frac{1}{2}\frac{N_{(a/b)}}{N_1}\left[F^{(1)}(x_0)\mathrm{Erfc}\left(\frac{y - y_0}{L_y}\right) \right.$$
$$\left. + F^{(1)}(x_0 + x^{(a/b)})\mathrm{Erfc}\left(\frac{y_0 - y}{L_y}\right) \right], \tag{A2}$$

where $N_{(a/b)}$ are the normalization constants, and $F^{(1)}$ is given in Eq. (6). The parameters $x^{(a)} = x_d$ and $x^{(b)} = (y - y_0)\cot(\theta)$ define the step segment along the y direction and the slanted step edge in the xy plane, respectively. Compared to the case of a single straight step, here there is an additional parameter in the form of the width of the error function along the y direction, L_y. We choose $L_y = L_x$, considering that the value of L_x has a negligible effect on the VO coupling.

3. Variational wave function: Two steps

In this Appendix we extend our formalism to the case of two parallel straight steps along the y direction. Defining the locations of the two steps at x_1 and x_2, we can now divide the interface into three regions $\mathcal{A}$, $\mathcal{B}$, and $\mathcal{C}$ with respective interface positions at $z = z_{\mathcal{A}}$, $z = z_{\mathcal{B}}$, and $z = z_{\mathcal{C}}$, as illustrated in Fig. 1. Based on the locations of each region, there are four possible configurations: the steps can form either upward or downward stairs, or rectangular terraces that can be either a bump or a dip. The Hamiltonian along the z direction for both stair and terrace configurations can be written as

$$H_z^{(2)} = H_z^{(0)}(z_{\mathcal{A}})\theta(x_1 - x) + H_z^{(0)}(z_{\mathcal{B}})\theta(x - x_1)$$
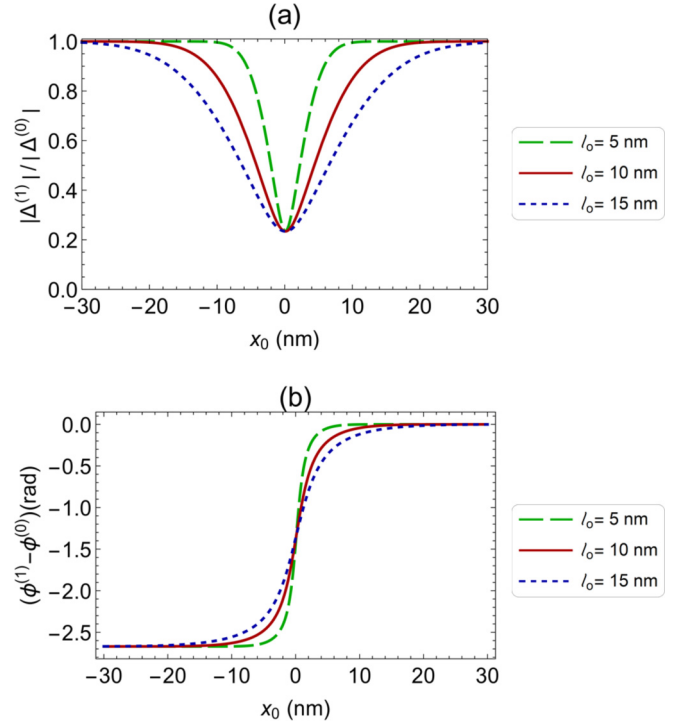$$\times \theta(x_2 - x) + H_z^{(0)}(z_{\mathcal{C}})\theta(x - x_2),$$

FIG. 15. Effect of in-plane quantum dot size on the magnitude and phase of VO coupling.

where $H_z^{(0)}(z_{\mathcal{A}})$, $H_z^{(0)}(z_{\mathcal{B}})$, and $H_z^{(0)}(z_{\mathcal{C}})$ are the Hamiltonians for regions $\mathcal{A}$, $\mathcal{B}$, and $\mathcal{C}$, with wave functions $\psi_{\mathcal{A}}(z)$, $\psi_{\mathcal{B}}(z)$, and $\psi_{\mathcal{C}}(z)$, respectively. Following the same procedure for the one-step case, the total wave function can now be written as

$$F^{(2)}(x, y, z) = \frac{N_2}{2}\phi(x, y)\left[\psi_{\mathcal{A}}(z)\,\mathrm{Erfc}\left(\frac{x - x_1}{L_x}\right) \right.$$
$$+ \frac{1}{2}\psi_{\mathcal{B}}(z)\,\mathrm{Erfc}\left(\frac{x_1 - x}{L_x}\right)\mathrm{Erfc}\left(\frac{x - x_2}{L_x}\right)$$
$$\left. + \psi_{\mathcal{C}}(z)\,\mathrm{Erfc}\left(\frac{x_2 - x}{L_x}\right) \right]. \tag{A3}$$

Here N_2 is the normalization constant, which depends on the locations of the steps at x_1 and x_2, and the width L_x of the complementary error function. Since the value of L_x is much smaller than the dimensions of the QD and does not affect the VO coupling strongly, we assume that the widths of the complementary error functions for the two steps are the same. We use the value of L_x (=1.5 nm), the same as in the single-step case.

APPENDIX B: EFFECT OF DOT SIZE ON VO COUPLING

The VO coupling results in the main text are all obtained assuming a QD radius of 10 nm. Within our vector model only the ratio of electron probability across a step is important; thus we do not expect any qualitative change in the step dependence for the VO coupling when QD size is varied. To verify this assertion, here we choose three different radii and calculate the phase and magnitude of VO coupling as functions of step location. We have chosen the same value of L_x for each radius. As shown in Fig. 15, the overall behavior of
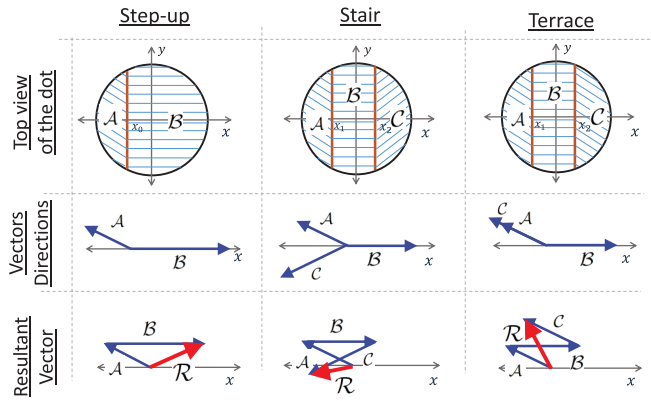
FIG. 16. Vector representation of the VO coupling for a single step, a two-step stair, and a rectangular terrace. We show the top view of the quantum dot in the first row; the vector representation of each shaded region and their resultant sum are shown in the second and third rows, respectively.

the magnitude and phase of VO coupling indeed remains the same. Quantitatively, for smaller dots the changes in both the magnitude and phase of VO coupling occur within a smaller length scale, and thus the rate of change increases when the dot size decreases, making VO coupling in a smaller quantum dot more sensitive to the location of an interface step.

APPENDIX C: VECTOR MODEL FOR VO COUPLING

As we discussed in the main text, our results on valley-orbit coupling can be explained in terms of vectors representing contributions from each step region. Here we provide a more detailed discussion of the vector model. In the following we label individual vectors in terms of the step regions they represent. After summing over all contributions, the resultant vector $\mathcal{R}$ corresponds to the total VO coupling. For illustration

we consider the cases of a single step, a two-step stair, and a rectangular terrace.

In the case of a single step, the step divides the QD into two regions labeled as $\mathcal{A}$ and $\mathcal{B}$. A top view with step position x_0 is shown in Fig. 16. The directions of the two vectors $\mathcal{A}$ and $\mathcal{B}$ are 0.85π and 0 from the x axis, respectively, as we choose region $\mathcal{B}$ to have $z_B = 0$ so that its contribution to VO coupling is real. Their magnitudes are proportional to the electron probability within the respective areas within the quantum dot. Clearly, the magnitude and direction of the resultant vector $\mathcal{R}$ depends on the location of the step. The magnitude of $\mathcal{R}$ reaches its minimum when the step location is at the center of the dot, so that vectors $\mathcal{A}$ and $\mathcal{B}$ are of equal length. The resultant vector $\mathcal{R}$ has a finite minimum magnitude and its direction varies from direction vector $\mathcal{B}$ to vector $\mathcal{A}$ as the step moves from left to right as shown in Fig. 16. The presence of a second step divides the quantum dot into three regions, as illustrated in Fig. 16. Here we consider two geometrical configurations, either two-stairs-up or a rectangular terrace. In both cases the directions of the vectors representing regions $\mathcal{A}$ and $\mathcal{B}$ are at 0.85π and 0 from the x axis, respectively, whereas the direction of $\mathcal{C}$ is -0.85π for the stairs-up case and 0.85π for the rectangular terrace. The different direction of the third vector for the stairs-up case means that the resultant vector $\mathcal{R}$ can cancel out completely. For a rectangular terrace, on the other hand, vectors $\mathcal{A}$ and $\mathcal{C}$ are parallel, so that the resultant vector $\mathcal{R}$ behaves in the same way as the case of a single step even though regions $\mathcal{A}$ and $\mathcal{C}$ are separated by $\mathcal{B}$ physically. Like in the one-step case, the minimum value of the VO coupling (or the minimum magnitude of vector $\mathcal{R}$) is reached when the electron probability splits equally between region $\mathcal{B}$ and the collective of regions $\mathcal{A}$ and $\mathcal{C}$, and region $\mathcal{B}$ does not necessarily lie at the center of the QD. The direction of the resultant vector $\mathcal{R}$ for both the stairs-up and terrace cases varies with the change in the contributions from vectors $\mathcal{A}$, $\mathcal{B}$, and $\mathcal{C}$. A final determination requires a more quantitative evaluation of the individual vectors, as we discussed in the main text.

[1] J. J. L. Morton, A. M. Tyryshkin, R. M. Brown, S. Shankar, B. W. Lovett, A. Ardavan, T. Schenkel, E. E. Haller, J. W. Ager, and S. A. Lyon, Nature (London) **455**, 1085 (2008).

[2] F. A. Zwanenburg, A. S. Dzurak, A. Morello, M. Y. Simmons, L. C. L. Hollenberg, G. Klimeck, S. Rogge, S. N. Coppersmith, and M. A. Eriksson, Rev. Mod. Phys. **85**, 961 (2013).

[3] G. Feher, R. C. Fletcher, and E. A. Gere, Phys. Rev. **100**, 1784 (1955).

[4] A. Morello, J. J. Pla, F. A. Zwanenburg, K. W. Chan, H. Huebl, M. Mottonen, C. D. Nugroho, C. Yang, J. A. van Donkelaar, A. D. C. Alves, D. N. Jamieson, C. C. Escott, L. C. L. Hollenberg, R. G. Clark, and A. S. Dzurak, Nature (London) **467**, 687 (2010).

[5] J. J. Pla, K. Y. Tan, J. P. Dehollain, W. H. Lim, J. J. L. Morton, D. N. Jamieson, A. S. Dzurak, and A. Morello, Nature (London) **489**, 541 (2012).

[6] J. Muhonen, J. Dehollain, A. Laucht, F. Hudson, T. Sekiguchi, K. Itoh, D. Jamieson, J. McCallum, A. Dzurak, and A. Morello, Nat. Nanotechnol. **9**, 986 (2014).

[7] M. Veldhorst, J. C. C. Hwang, C. H. Yang, A. Leenstra, B. de Ronde, J. P. Dehollain, J. T. Muhonen, F. E. Hudson, K. M. Itoh, A. Morello, and A. S. Dzurak, Nat. Nanotechnol. **9**, 981 (2014).

[8] D. M. Zajac, T. M. Hazard, X. Mi, K. Wang, and J. R. Petta, Appl. Phys. Lett. **106**, 223507 (2015).

[9] G. Burkard and J. R. Petta, Phys. Rev. B **94**, 195305 (2016).

[10] X. Mi, C. G. Péterfalvi, G. Burkard, and J. R. Petta, Phys. Rev. Lett. **119**, 176803 (2017).

[11] M. Russ, D. M. Zajac, A. J. Sigillito, F. Borjans, J. M. Taylor, J. R. Petta, and G. Burkard, Phys. Rev. B **97**, 085421 (2018).

[12] D. Zajac, A. Sigillito, M. Russ, F. Borjans, J. Taylor, G. Burkard, and J. Petta, Science **359**, 439 (2018).

[13] K. Takeda, J. Kamioka, T. Otsuka, J. Yoneda, T. Nakajima, M. R. Delbecq, S. Amaha, G. Allison, T. Kodera, S. Oda, and S. Tarucha, Sci. Adv. **2**, e1600694 (2016).

[14] J. Yoneda, K. Takeda, T. Otsuka, T. Nakajima, M. R. Delbecq, G. Allison, T. Honda, T. Kodera, S. Oda, Y. Hoshi, N.

Usami, K. M. Itoh, and S. Tarucha, Nat. Nanotechnol. **13**, 102 (2018).

[15] B. M. Maune, M. G. Borselli, B. Huang, T. D. Ladd, P. W. Deelman, K. S. Holabird, A. A. Kiselev, I. Alvarado-Rodriguez, R. S. Ross, A. E. Schmitz, M. Sokolich, C. A. Watson, M. F. Gyure, and A. T. Hunter, Nature (London) **481**, 344 (2012).

[16] K. Eng, T. D. Ladd, A. Smith, M. G. Borselli, A. A. Kiselev, B. H. Fong, K. S. Holabird, T. M. Hazard, B. Huang, P. W. Deelman, I. Milosavljevic, A. E. Schmitz, R. S. Ross, M. F. Gyure, and A. T. Hunter, Sci. Adv. **1**, e1500214 (2015).

[17] M. Friesen, M. A. Eriksson, and S. N. Coppersmith, Appl. Phys. Lett. **89**, 202106 (2006).

[18] M. Friesen, S. Chutia, C. Tahan, and S. N. Coppersmith, Phys. Rev. B **75**, 115318 (2007).

[19] M. Friesen and S. N. Coppersmith, Phy. Rev. B **81**, 115324 (2010).

[20] J. K. Gamble, M. A. Eriksson, S. N. Coppersmith, and M. Friesen, Phys. Rev. B **88**, 035310 (2013).

[21] P. Scarlino, E. Kawakami, D. R. Ward, D. E. Savage, M. G. Lagally, M. Friesen, S. N. Coppersmith, M. A. Eriksson, and L. M. K. Vandersypen, Phys. Rev. Lett. **115**, 106802 (2015).

[22] D. Kim, D. R. Ward, C. B. Simmons, D. E. Savage, M. G. Lagally, M. Friesen, S. N. Coppersmith, and M. A. Eriksson, npj Quantum Inf. **1**, 15004 (2015).

[23] R. Ferdous, E. Kawakami, P. Scarlino, M. P. Nowak, D. R. Ward, D. E. Savage, M. G. Lagally, S. N. Coppersmith, M. Friesen, and M. A. Eriksson *et al.*, npj Quantum Inf. **4**, 26 (2018).

[24] J. C. Abadillo-Uriel, B. Thorgrimsson, D. Kim, L. W. Smith, C. B. Simmons, D. R. Ward, R. H. Foote, J. Corrigan, D. E. Savage, M. G. Lagally, M. J. Calderón, S. N. Coppersmith, M. A. Eriksson, and M. Friesen, Phys. Rev. B **98**, 165438 (2018).

[25] T. Ando, A. B. Fowler, and F. Stern, Rev. Mod. Phys. **54**, 437 (1982).

[26] C. H. Yang, A. Rossi, R. Ruskov, N. S. Lai, F. A. Mohiyaddin, S. Lee, C. Tahan, G. Klimeck, A. Morello, and A. S. Dzurak, Nat. Commun. **4**, 2069 (2013).

[27] J. K. Gamble, P. Harvey-Collard, N. T. Jacobson, A. D. Baczewski, E. Nielsen, L. Maurer, I. Montaño, M. Rudolph, M. S. Carroll, C. H. Yang, A. Rossi, A. S. Dzurak, and R. P. Muller, Appl. Phys. Lett. **109**, 253101 (2016).

[28] M. Veldhorst, H. G. J. Eenink, C. H. Yang, and A. S. Dzurak, Nat. Commun. **8**, 1766 (2017).

[29] D. Culcer, L. Cywiński, Q. Li, X. Hu, and S. Das Sarma, Phy. Rev. B **82**, 155312 (2010).

[30] D. Culcer, X. Hu, and S. Das Sarma, Phy. Rev. B **82**, 205315 (2010).

[31] N. M. Zimmerman, P. Huang, and D. Culcer, Nano Lett. **17**, 4461 (2017).

[32] A. L. Saraiva, M. J. Calderón, X. Hu, S. Das Sarma, and B. Koiller, Phys. Rev. B **80**, 081305(R) (2009).

[33] A. L. Saraiva, M. J. Calderón, R. B. Capaz, X. Hu, S. Das Sarma, and B. Koiller, Phys. Rev. B **84**, 155320 (2011).

[34] Y. Wu and D. Culcer, Phys. Rev. B **86**, 035321 (2012).

[35] P. Boross, G. Szèchenyi, D. Culcer, and A. Pàlyi, Phys. Rev. B **94**, 035438 (2016).

[36] P. Huang and X. Hu, Phys. Rev. B **90**, 235315 (2014).

[37] W. Huang, M. Veldhorst, N. M. Zimmerman, A. S. Dzurak, and D. Culcer, Phys. Rev. B **95**, 075403 (2017).

[38] T. B. Boykin, G. Klimeck, M. Friesen, S. N. Coppersmith, P. von Allmen, F. Oyafuso, and S. Lee, Phys. Rev. B **70**, 165325 (2004).

[39] M. O. Nestoklon, L. E. Golub, and E. L. Ivchenko, Phys. Rev. B **73**, 235334 (2006).

[40] T. B. Boykin, N. Kharche, and G. Klimeck, Phys. Rev. B **77**, 245320 (2008).

[41] S. Srinivasan, G. Klimeck, and L. P. Rokhinson, Appl. Phys. Lett. **93**, 112102 (2008).

[42] R. Ferdous, K. W. Chan, M. Veldhorst, J. C. C. Hwang, C. H. Yang, H. Sahasrabudhe, G. Klimeck, A. Morello, A. S. Dzurak, and R. Rahman, Phys. Rev. B **97**, 241401(R) (2018).

[43] L. Bourdet and Y.-M. Niquet, Phys. Rev. B **97**, 155433 (2018).

[44] X. Zhao and X. Hu, arXiv:1803.00749.

[45] T. A. Baart, N. Jovanovic, C. Reichl, W. Wegscheider, and L. M. K. Vandersypen, Appl. Phys. Lett. **109**, 043101 (2016).

[46] H. Flentje, B. Bertrand, P. Mortemousque, A. Ludwig, A. D. Wieck, C. Bäuerle, and T. Meunier, Appl. Phys. Lett. **110**, 233101 (2017).

[47] T. Fujita, T. A. Baart, C. Reichl, W. Wegscheider, and L. M. K. Vandersypen, npj Quantum Inf. **3**, 22 (2017).

[48] A. R. Mills, D. M. Zajac, M. J. Gullans, F. J. Schupp, T. M. Hazard, and J. R. Petta, Nat. Commun. **10**, 1063 (2019).

[49] P.-A. Mortemousque, E. Chanrion, B. Jadot, H. Flentje, A. Ludwig, A. D. Wieck, M. Urdampilleta, C. Bauerle, and T. Meunier, arXiv:1808.06180.

[50] A. R. Mills, M. M. Feldman, C. Monical, P. J. Lewis, K. W. Larson, A. M. Mounce, and J. R. Petta, Appl. Phys. Lett. **115**, 113501 (2019).

[51] J. R. Petta, A. C. Johnson, C. M. Marcus, M. P. Hanson, and A. C. Gossard, Phys. Rev. Lett. **93**, 186802 (2004).

[52] Z. Shi, C. B. Simmons, J. R. Prance, J. K. Gamble, T. S. Koh, Y.-P. Shim, X. Hu, D. E. Savage, M. G. Lagally, M. A. Eriksson, M. Friesen, and S. N. Coppersmith, Phys. Rev. Lett. **108**, 140503 (2012).

[53] D. Culcer, A. L. Saraiva, B. Koiller, X. Hu, and S. Das Sarma, Phys. Rev. Lett. **108**, 126804 (2012).

[54] T. Kobayashi, J. van der Heijden, M. G. House, S. J. Hile, P. Asshoff, M. F. Gonzalez-Zalba, M. Vinet, M. Y. Simmons, and S. Rogge, Appl. Phys. Lett. **108**, 152102 (2016).

[55] X. Mi, J. V. Cady, D. M. Zajac, P. W. Deelman, and J. R. Petta, Science **355**, 156 (2017).

[56] G. Burkard, D. Loss, and D. P. DiVincenzo, Phys. Rev. B **59**, 2070 (1999).

[57] X. Hu and S. Das Sarma, Phys. Rev. A **61**, 062301 (2000).

[58] L. Jiang, C. H. Yang, Z. Pan, A. Rossi, A. S. Dzurak, and D. Culcer, Phys. Rev. B **88**, 085311 (2013).

[59] M. L. V. Tagliaferri, P. L. Bavdaz, W. Huang, A. S. Dzurak, D. Culcer, and M. Veldhorst, Phys. Rev. B **97**, 245412 (2018).

[60] G. Bastard, *Wave Mechanics Applied to Semiconductor Heterostructures* (Halsted, New York, 1988).

[61] M. Abramowitz and I. A. Stegun, editors, *Handbook of Mathematical Functions with Formulas, Graphs, and Mathematical Tables*, 9th printing (Dover, New York, 1972), pp. 299–300.

[62] S. N. Filimonov and B. Voigtländer, Surf. Sci. **549**, 31 (2004).

[63] B. Koiller, R. B. Capaz, X. Hu, and S. Das Sarma, Phys. Rev. B **70**, 115207 (2004).

[64] J. Myslivecek, C. Schelling, F. Schäffler, G. Springholz, P. Smilauer, J. Krug, and B. Voigtländer, Surf. Sci. **520**, 193 (2002).

[65] S. Goswami, K. A. Slinker, M. Friesen, L. M. McGuire, J. L. Truitt, C. Tahan, L. J. Klein, J. O. Chu, P. M. Mooney, D. W. Van Der Weide, R. Joynt, S. N. Coppersmith, and M. A. Eriksson, Nat. Phys. **3**, 41 (2007).

[66] D. J. Griffiths, *Introduction to Quantum Mechanics*, 2nd ed. (Pearson Prentice Hall, Upper Saddle River, NJ, 2004).